Yu, X., Yuan, Z., Li, H., Huang, S., Wang, D., Yao, F., Funsten, H. O., Wygant, J. R. (2018): Response of Banded Whistler Mode Waves to the Enhancement of Solar Wind Dynamic Pressure in the Inner Earth's Magnetosphere. - *Geophysical Research Letters*, *45*, 17, pp. 8755—8763.

DOI: http://doi.org/10.1029/2018GL078849

Geophysical Research Letters

RESEARCH LETTER
10.1029/2018GL078849

Key Points:
- This paper provides in situ evidence of local excitation of broadband whistler mode waves outside plasmapause in the inner magnetosphere
- The normalized frequencies of broadband whistler waves become higher with enhancements of the solar wind pressure
- This paper has revealed the frequency properties of broadband whistler mode waves by solar wind dynamic pressure enhancements

Supporting Information:
- Supporting Information S1

Correspondence to:
Z. Yuan,
y_zgang@vip.163.com

Citation:
Yu, X., Yuan, Z., Li, H., Huang, S., Wang, D., Yao, F., et al. (2018). Response of banded whistler mode waves to the enhancement of solar wind dynamic pressure in the inner Earth's magnetosphere. *Geophysical Research Letters*, *45*, 8755–8763. https://doi.org/10.1029/2018GL078849

Received 19 MAY 2018
Accepted 20 AUG 2018
Accepted article online 27 AUG 2018
Published online 10 SEP 2018

Response of Banded Whistler Mode Waves to the Enhancement of Solar Wind Dynamic Pressure in the Inner Earth's Magnetosphere

Xiongdong Yu[1], Zhigang Yuan[1], Haimeng Li[2], Shiyong Huang[1], Dedong Wang[3], Fei Yao[1], H. O. Funsten[4], and J. R. Wygant[5]

[1]School of Electronic Information, Wuhan University, Wuhan, China, [2]Institute of Space Science and Technology, Nanchang University, Nanchang, China, [3]GFZ German Research Center for Geosciences, Potsdam, Germany, [4]ISR Division, Los Alamos National Laboratory, Los Alamos, NM, USA, [5]School of Physics and Astronomy, University of Minnesota, Minneapolis, MN, USA

Abstract With observations of Van Allen Probe A, in this letter we display a typical event where banded whistler waves shifted up their frequencies with frequency bands broadening as a response to the enhancement of solar wind dynamic pressure. Meanwhile, the anisotropy of electrons with energies about several tens of keV was observed to increase. Through the comparison of the calculated wave growth rates and observed wave spectral intensity, we suggest that those banded whistler waves observed with frequencies shifted up and frequency bands broadening could be locally excited by these hot electrons with increased anisotropy. The current study provides a great in situ evidence for the influence on frequencies of banded whistler waves by the enhancement of solar wind dynamic pressures, which reveals the important role of solar wind dynamic pressures playing in the frequency properties of banded whistler waves.

Plain Language Summary In the inner magnetosphere, broadband whistler waves are often taken into account in understanding the evolution of the Earth's radiation belts. Solar wind dynamic pressures, as a driving factor, can influence whistler-mode waves not only on their occurrence, but also on their frequencies. However,the proof for the influence of the solar wind pressure on the frequency properties of the excited banded whistler waves in the inner magnetosphere has not been uncovered.With observations of Van Allen Probe A, we display a typical event that broadband whistler waves can be locally excited as a response to the enhancement of solar wind dynamic pressure. As the solar wind pressure enhanced, the normalized frequencies of broadband whistler waves became higher. Through the comparison of the calculated wave growth rates and observed wave spectral intensity, we suggest that broadband whistler waves could be locally excited with higher frequencies by these hot electrons with increased anisotropy. The current study provides a great in situ evidence for the influence on frequencies of banded whistler waves by the enhancement of solar wind dynamic pressures, which reveals the important role of solar wind dynamic pressures playing in the frequency properties of banded whistler waves.

1. Introduction

Whistler mode waves are one of the most common plasma emissions in the Earth's magnetosphere (Bortnik et al., 2008; Huang et al., 2016, 2017; Li, Thorne, Angelopoulos, Bortnik, et al., 2009; Meredith et al., 2004; Thorne et al., 1974), and other magnetized plasma environments of astrophysical objects (Gurnett et al., 1996; Horne et al., 2008; Russell et al., 2007). Especially, whistler mode waves are found to be rich in the inner magnetosphere of the Earth. These waves have been demonstrated to be capable of effectively accelerating electrons in the Earth's radiation belts (S. Liu et al., 2015; N. Liu et al., 2017; Shprits et al., 2013; Summers et al., 2002; Thorne et al., 2013; Xiao et al., 2009, 2010, 2014, 2015; Yang et al., 2018), as well as causing energetic electrons to precipitate into the ionosphere (Summers et al., 2008; Thorne et al., 2010). Radiation belt electrons with relativistic energies can make damage to spacecraft and astronauts in space; it is thus of importance to study and understand the generation of whistler mode waves.

In Earth's inner magnetosphere, whistler mode waves in the plasmasphere, called as plasmaspheric hiss waves, are observed to be unstructured (Bortnik et al., 2008; Cornilleau-wehrlin et al., 1993; Thorne et al., 1973; Yuan et al., 2012), while outside the plasmapause, two kinds of whistler mode waves are often found:

chorus waves and banded whistler waves (e.g., K. Liu et al., 2011; Santolík et al., 2003). The former is usually composed of fine structures (rising tone or/and falling tone elements), while the latter is unstructured so that these waves are sometimes called hiss-like whistler mode emissions (Gao et al., 2014; Li et al., 2012), or exo-hiss (Bortnik et al., 2008; N. Liu et al., 2017). The plasmaspheric hiss waves are proposed to originate from the chorus waves outside the plasmapause (Bortnik et al., 2008). Additionally, temperature-anisotropy electrons, with energies of several keV to several tens of keV, have been demonstrated to be a potential candidate for local excitation of whistler waves outside the plasmapause (e.g., Gao et al., 2016; Kennel & Petschek, 1966; K. Liu et al., 2011; Su et al., 2014; Xiao et al., 2006). Generally, electrons would evolve anisotropic temperatures after injected from the plasma sheet into the inner magnetosphere, and the whistler mode instabilities can thus be excited (Li et al., 2008; Li, Thorne, Angelopoulos, Bonnell, et al., 2009). On the other hand, magnetospheric compression resulting from the enhancement of solar wind pressure has been proposed to be another alternative to developing temperature-anisotropic electrons, which is responsible for the generation of chorus waves in the dayside outer magnetosphere (e.g., Fu et al., 2012; Li, Thorne, Angelopoulos, Bortnik, et al., 2009; Tsurutani & Smith, 1977), but the influence of the solar wind pressure on the frequency properties of the excited banded whistler waves outside the plasmapause in the inner magnetosphere has not been uncovered.

In this letter, we report a typical event occurred in 16 February 2014, in which case banded whistler waves shifted their frequencies as a response to the enhancement of solar wind dynamic pressures. Using in situ data provided by the Van Allen Probe A, we show that as solar wind dynamic pressure increased, the temperature anisotropy of electrons increased correspondingly, and, as a result, banded whistler waves could be locally excited with higher frequencies. It is demonstrated from our results that the enhancement of solar wind dynamic pressures could make an important effect to banded whistler waves not only on their occurrence but also on their frequencies as well as frequency bands.

2. Observations

The National Aeronautics and Space Administration mission, Van Allen Probes, consisting of two identically spacecraft, has been orbiting the Earth's magnetosphere near the equatorial plane since launched in August 2012 (Mauk et al., 2013). In this letter, we use the wave spectrum data, obtained from the Electric and Magnetic Field Instrument Suite and Integrated Science Waves instrument (Kletzing et al., 2013), and particle data attained from the Helium, Oxygen, Proton, and Electron Mass Spectrometer (Funsten et al., 2013). Additionally, the plasma density data are derived from the upper hybrid resonant frequencies (Kurth et al., 2015).

Figure 1 shows the overview of the typical event observed by Van Allen Probe A during 1100 UT to 1400 UT on 16 February 2014. During this interval, chorus waves are observed near 0.5 f_{ce} (the solid white curve in Figure 1c) with right-hand polarizations and moderate wave normal angles, that is, $\varepsilon \sim 1$ and $\theta \sim 50°$, while the banded whistler waves, having right-hand polarizations ($\varepsilon \sim 1$) but small wave normal angles ($\theta \sim 0°$), are observed with center frequencies during 500–1,000 Hz. During the time interval of interest, there occurred three successive events of solar wind dynamic pressure (P_{sw}) enhancements (Figure 1a), each of which is followed by an increase of *SYM-H* index (Figure 1b). Note that the data for the second P_{sw} enhancement is sparse, but we can identify it in virtue of the increase of *SYM-H* index in Figure 1b. In the meanwhile, the frequencies of banded whistler waves were accordingly shifted up after each P_{sw} enhancement. Especially, as a response of the first enhancement of P_{sw} at about 1220 UT, the frequencies of banded whistler waves were shifted from about 500 Hz up to about 1,000 Hz. Note that there are time lags between the P_{sw} enhancement and the increase of *SYM-H* as well as wave frequencies. This is because that the latter is observed inside the magnetosphere, while the enhancement of P_{sw} is observed outside the magnetosphere.

On the other hand, as shown in Figure 2, the local magnetic field intensity B_t increased (Figure 2c) due to the compression of the magnetosphere by the solar wind pressure, while thermal electrons are energized up to about 5 keV (Figure 2d), which might result from conservation of magnetic moment (proportional to the ratio of the particle energy transverse to the magnetic field to the magnetic field intensity). Moreover, the observed background plasma density N_e (Figure 2b) indicates that there was no obvious plasma boundary observed, which also confirms that these changes of the local plasma environment are owing to the enhancement of P_{sw}, rather than to that satellite has passed through different plasma regions. To make further study the frequency changes of band whistler waves, we have calculated the normalized

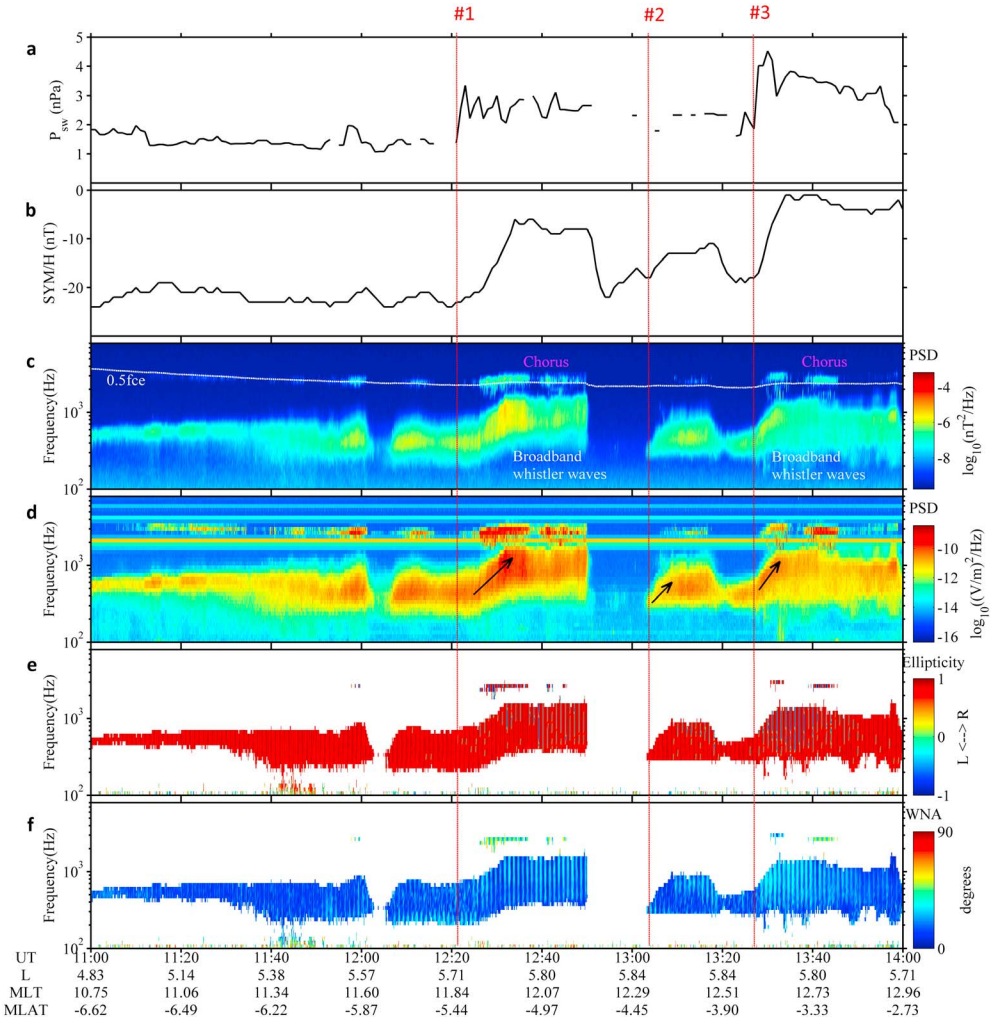

Figure 1. Overview of typical event occurred in 16 February 2014. (a and b) Solar wind dynamic pressure and *SYM-H* index. (c and d) Magnetic spectral intensity and electric spectral intensity observed by Electric and Magnetic Field Instrument Suite and Integrated Science instrument. (e) Wave ellipticity, the degree of elliptical polarization. (f) Wave normal angles, the angles between the background magnetic field, and the wave vectors. PSD = power spectral density.

frequencies X through dividing the frequencies f_0 of the peak wave power spectral density (PSD) by the electron gyrofrequencies (f_{ce}), that is, $X = f_0/f_{ce}$. It is clearly shown in Figure 2f that the normalized frequencies of the observed banded whistler waves were blow 0.1 ($X < 0.1$) before the enhancement of P_{sw} but increased up to 0.2 ($X \sim 0.2$) after P_{sw} enhancement. Note that Van Allen Probe B has observed the similar frequency response of banded whistler waves at the same time (not shown), which indicates that the frequency response of banded whistler waves to the enhancement of solar wind dynamic pressures might occur over a wide region. Since similar observations are resulted for three enhancement events, we will focus only on the first event in the following.

To investigate this event more in details, we have checked the burst mode data of wave field during the time interval of interest. As a result, the available high-resolution wave PSD at about 1211UT (before P_{sw} enhancement) and about 1244UT (after P_{sw} enhancement) are shown in Figures 3a and 3b, respectively. As shown in both panels, banded whistler waves are observed to be separated from the whistler mode chorus waves. The latter are identified as the precise falling tone structures (Li et al., 2011; Omura et al., 2008) just below and above 0.5 f_{ce} (the solid white curves), resulting from nonlinear processes between whistler waves and electrons (Omura et al., 2008), while the former have incoherent structures and have their frequencies shifted from about 500 Hz (Figure 3a) up to about 1,000 Hz (Figure 3b), which is the focus of this letter. It is worth

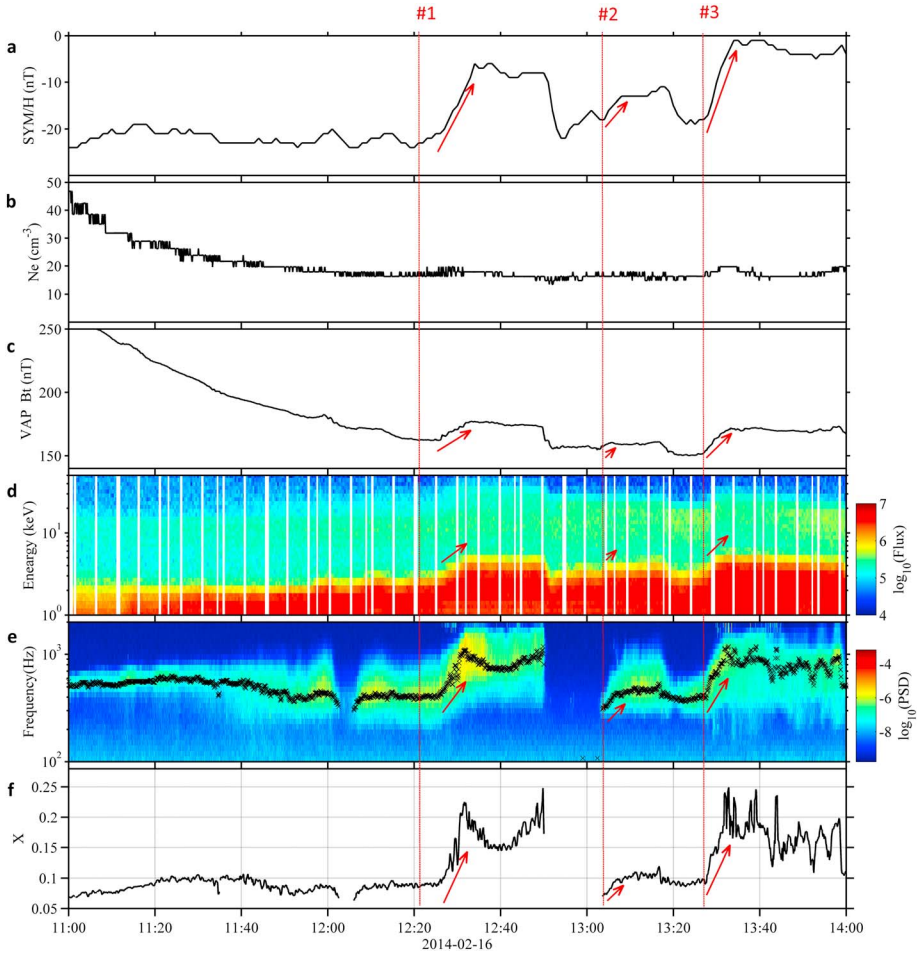

Figure 2. In situ plasma environment between 1100 UT and 1400 UT. (a–d) *SYM-H* index, measured plasma density, magnetic field intensity, and electron flux. (e) Magnetic spectral intensity, with the black asterisk denoting the abstracted wave frequencies (f_0) corresponding to the maximum spectral intensity. (f) Normalized wave frequencies $X = f_0/f_{ce}$. PSD = power spectral density.

noting that the frequency bands of banded whistler waves have also become much broader. The low-electron density ($<$20 cm^3 in Figure 2b) and coexisting chorus waves mean that the banded whistler waves were observed outside the plasmapause in the inner magnetosphere. Moreover, the electron velocity distributions in different energy levels observed at about 1211 UT (denoted as dots) and 1244 UT (denoted as circles) are displayed as a function of pitch angle α (the angle between electron velocity and the background magnetic field) in Figure 3c, respectively. It is clearly shown that as a result of P_{sw} enhancement, electrons are energized mostly in the direction normal to the background magnetic field (α = 90°), especially for electrons with energies between 24 and 37 keV, implying an increase of the temperature anisotropy for these electrons. These hot temperature-anisotropy electrons are suggested to be able to drive the instability for whistler wave generations (e.g., Kennel & Petschek, 1966).

3. Discussion

One common and effective method of studying wave generation is to inspect the linear growth rate driven by unstable particle phase space distributions (Chen et al., 2010; Kennel & Petschek, 1966; Yu et al., 2016, 2018; Yuan et al., 2017). For a given wave frequency, positive growth rate indicates the possibility for wave excitation, while negative growth rate would result in wave damping. To calculate linear growth rate, the measured electron velocity distributions before and after P_{sw} enhancement have been optimally fitted with multicomponent distributions as described in Yu et al. (2016, 2018), and the fitted parameter sets are

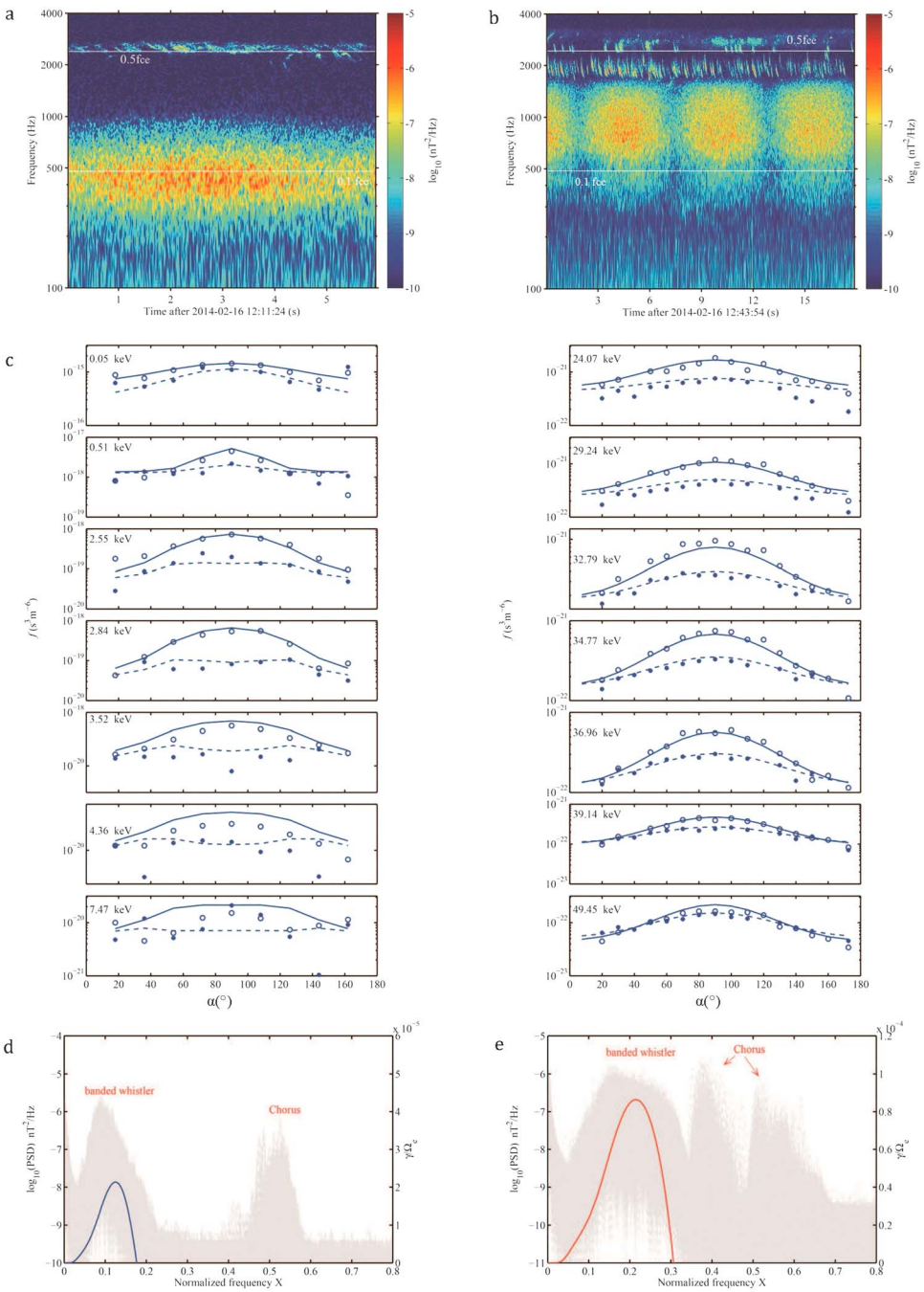

Figure 3. Linear wave growth rates γ based on the measured electron distributions. Dynamic spectrum of burst mode magnetic field data at (a) about 1211 UT (before the first P_{sw} enhancement event) and (b) about 1244 UT (after the first P_{sw} enhancement event). (c) Electron velocity distributions in different energy levels observed at about 1211 UT (denoted as dots) and 1244 UT (denoted as circles) as a function of pitch angle α. The dashed and solid curves denote the fitted distributions at 1211 UT and 1244 UT, respectively. (d and e) Comparison of the observed wave power spectral density (PSD) and the calculated growth rate at 1211 UT and 1244 UT, respectively.

illustrated in Tables 1 and 2, respectively. The fitted distributions before and after P_{sw} enhancement have also been displayed as in dashed and solid curves in Figure 3c, respectively. Additionally, we assume that the plasma environment is only composed of protons and electrons. The protons are assumed to have a cold Maxwellian distribution with a temperature of 2 eV and a density equating to the measured plasma density, while cold electrons having a temperature of 0.6 eV are included to keep charge neutrality (Horne

Table 1
Electron Components Used to Model the Electron Distributions Observed at About 12:11:20 UT, When N_e is 16.5 cm^{-3} and Bt is 171.5 nT

Components	n (cm^{-3})	$T_{//}$ (eV)	$T_{\perp}$ (eV)	E_r (eV)[a]
1	2.000	10.5	13.0	0
2	0.250	40	80	0
3	0.030	280	70	1.38×10^3
4	0.050	400	400	0
5	0.015	4.4×10^3	4.4×10^3	0
6	0.005	11×10^3	16×10^3	0
7	0.001	36×10^3	45×10^3	0

[a] $E_r = \frac{1}{2} m_h V_r^2$ is the energy parameter relative to the ring speed V_r (Yu et al., 2016).

& Thorne, 1993; Olsen et al., 1987). Moreover, since the density of the observed electrons is much smaller than that of the cold plasma, and the calculated growth rates are much smaller than the wave frequency (cf. Figures 3e and 3f), it is valid to use the cold plasma dispersion relation as an approximation for the real part of the kinetic dispersion relation (Kennel & Petschek, 1966; Yu et al., 2016).

With the fitted distributions as well as the observed background plasma density (Figure 2b) and magnetic field (Figure 2c), the calculation of the linear growth rates for whistler mode waves before and after P_{sw} enhancement has been performed. The results have been shown as the blue curve in Figure 3d and the red curve in Figure 3e, respectively. Meanwhile, the observed wave PSD before and after P_{sw} enhancement (Figures 3a and 3b) have also been illustrated as gray curves in Figures 3d and 3e for comparison. As shown in Figures 3d and 3e, before P_{sw} enhancement, the frequency band of the instability indicated by positive growth rate is roughly consistent with the observed wave frequency band, but the frequency of the peak growth rate is different from that of the peak wave PSD. This inconsistency between the theoretical calculation and wave observations might be due to that before being observed by the satellite, the initial distributions of electrons driving the whistler wave instability have evolved significantly as the wave grows. After the sudden enhancement of P_{sw}, the distributions of hot electrons become more temperature-anisotropic. According to the linear wave growth theory (e.g., Kennel & Petschek, 1966), these electrons with temperature-anisotropy distributions would drive the growth of whistler waves shifting to higher normalized frequencies. This frequency shift has been confirmed by the consistency of the calculated grow rate and the observed waves PSD, in both peak and frequency band. Therefore, it is suggested that the banded whistler waves can be locally excited by hot electrons with temperature anisotropy. As temperature anisotropy increases resulting from P_{sw} enhancement, hot electrons drive whistler waves with a higher-frequency and a broader-frequency band, indicating the important role of the solar wind pressure playing in frequency properties of the banded whistler waves in the inner magnetosphere.

In supporting information S1, we have also calculated the wave growth rate for the third enhancement event of P_{sw} and compared the result with that for the first enhancement event. It is shown that because the solar wind dynamic pressure increased a little more in the third enhancement event, the frequency band of both the observed banded whistler waves and the calculated growth rate have become broader, as compared to those in the first enhancement event. This comparison provides a strong support for that solar wind dynamic pressures can make effects in the frequency properties of banded whistler waves.

In fact, wave PSD and particle distributions will develop as wave grows. As shown in Figure 2 in Seough and Yoon (2012), when the amplitude of waves is small, the effect of waves on particles is negligible, and thus, the wave spectrum would be consistent with the growth rate driven by particle distributions (see the first column from left), which also indicates that wave growth is in the linear growth stage and near the initial state. As wave grows, diffusion of particles resulting from waves will become more and more significant, and apparent development of particle distributions would occur. Accordingly, the growth rate changes (see the second and third column from left), including the peak value and its corresponding frequency. Finally, wave spectrums and particle distributions will reach the saturation state, in which wave spectrums would generally not be consistent with the growth rate (see the fourth column from left). Note that in their case, the frequency corresponding to the peak growth rate in the saturation is greater than that corresponding to the peak wave spectrum. In our cases, the wave spectrum and calculated growth rate before P_{sw} enhancement (at about 1211 UT) are similar to those shown in the fourth column of Figure 2 in Seough and Yoon (2012), which indicates that these observed waves and particles are in/near the saturation state. As for the disagreement between linear growth rate profile and wave spectrums shown in Figure 3d, in general it is also possibly resulted from the low time resolution of the observed electron distribution data, which is due to an average in the observed duration.

Table 2
The Same As Table 1 But at About 12:44:04 UT, When N_e is 16.3 cm^{-3} and Bt is 174.5 nT

Components	n (cm^{-3})	$T_{//}$ (eV)	$T_{\perp}$ (eV)	E_r (eV)
1	2.000	11.5	14.0	0
2	0.300	40	110	0
3	0.030	920	410	2.08×10^3
4	0.050	600	600	0
5	0.010	2.0×10^3	2.0×10^3	0
6	0.015	7.1×10^3	11×10^3	0
7	0.0016	28×10^3	42×10^3	0

In fact, for our cases, solar wind dynamic pressures have sustained in a low level for a long time (at least an hour) before the first enhancement event (cf. Figure 1a), suggesting that wave spectrums and electrons distributions might have sufficiently developed. Since wave spectrums and particle distributions would not have significant changes when it comes into the saturation stage, the averaged distributions might not make important influence on the calculation of growth rates in our cases. In addition, even if the banded whistler waves observed before the enhancement event are in the linear stage, they would finally develop into ones with lower normalized frequencies (shown in Figure 3d), which would make negligible influence on our conclusions. On the other hand, as shown in Figure 3e, the wave spectrum and calculated growth rate after P_{sw} enhancement (at about 1244 UT) are more similar to those shown in the first and/or second column of Figure 2 in Seough and Yoon (2012), which indicates that waves and particles observed at this time interval are in the linear growth stage, and at/near the initial state. To make the full process of wave growth and saturations more clearly in observations, the time resolution of the data used here is too low and advanced satellite data with a higher time resolution should be used. The detailed analysis of the evolution process is beyond the scope of the letter, which will be investigated in the future work.

4. Conclusion

In presented calculations we provide a further confirmation of the local excitation of banded whistler mode waves by the in situ hot temperature-anisotropy electrons. As solar wind dynamic pressure increased, the temperature anisotropy of electrons increased correspondingly, and as a result, banded whistler waves could be locally excited with higher-frequencies and broader-frequency bands. Therefore, this letter provides a direct in situ evidence for the influence on frequencies of banded whistler waves by the enhancement of solar wind dynamic pressures and reveals the important role of the solar wind pressure playing in the frequency properties of banded whistler waves. This excitation mechanism is universal, and similar excitation should be found for other wave emissions in terrestrial magnetosphere and other magnetic plasma environments in space.

It should be mentioned that throughout this study, we use the linear growth theory in our approach to the wave generation. The linear growth theory has been frequently adopted in treatment with wave excitation, though nonlinear wave particle interactions have been proposed to be an alternative for wave growth (Omura et al., 2008; Summers et al., 2011). The conclusions here drawn from the linear wave growth are expected to be a basis for future research using nonlinear approaches.

Acknowledgments
We acknowledge the Van Allen Probes data from the EMFISIS and HOPE instrument obtained from http://emfisis.physics.uiowa.edu/data/index, and http://www.rbsp-ect.lanl.gov/data_pub/, respectively. We thank Craig A. Kletzing for providing the data of the EMFISIS and advice on their usage. This work is supported by the National Natural Science Foundation of China (41374168, 41521063, 41604156, and 41874194) and Program for New Century Excellent Talents in University (NCET-13-0446).

References

Bortnik, J., Thorne, R. M., & Meredith, N. P. (2008). The unexpected origin of plasmaspheric hiss from discrete chorus emissions. *Nature*, *452*(7183), 62–66. https://doi.org/10.1038/nature06741

Chen, L., Thorne, R. M., Jordanova, V. K., & Horne, R. B. (2010). Global simulation of magnetosonic wave instability in the storm time magnetosphere. *Journal of Geophysical Research*, *115*, A11222. https://doi.org/10.1029/2010JA015707

Cornilleau-Wehrlin, N., Solomon, J., Korth, A., & Kremser, G. (1993). Generation mechanism of plasmaspheric ELF/VLF hiss: A statistical study from GEOS 1 data. *Journal of Geophysical Research*, *98*(A12), 21,471–21,479. https://doi.org/10.1029/93JA01919

Fu, H. S., Cao, J. B., Mozer, F. S., Lu, H. Y., & Yang, B. (2012). Chorus intensification in response to interplanetary shock. *Journal of Geophysical Research*, *117*, A01203. https://doi.org/10.1029/2011JA016913

Funsten, H. O., Skoug, R. M., Guthrie, A. A., MacDonald, E. A., Baldonado, J. R., Harper, R. W., et al. (2013). Helium, Oxygen, Proton, and Electron (HOPE) mass spectrometer for the Radiation Belt Storm Probes mission. *Space Science Reviews*, *179*(1–4), 423–484. https://doi.org/10.1007/s11214-013-9968-7

Gao, X., Li, W., Thorne, R. M., Bortnik, J., Angelopoulos, V., Lu, Q., et al. (2014). New evidence for generation mechanisms of discrete and hiss-like whistler mode waves. *Geophysical Research Letters*, *41*, 4805–4811. https://doi.org/10.1002/2014GL060707

Gao, X., Lu, Q., Bortnik, J., Li, W., Chen, L., & Wang, S. (2016). Generation of multiband chorus by lower band cascade in the Earth's magnetosphere. *Geophysical Research Letters*, *43*, 2343–2350. https://doi.org/10.1002/2016GL068313

Gurnett, D. A., Kurth, W. S., Roux, A., Bolton, S. J., & Kennel, C. F. (1996). Evidence for a magnetosphere at Ganymede from plasma-wave observations by the Galileo spacecraft. *Nature*, *384*(6609), 535–537. https://doi.org/10.1038/384535a0

Horne, R. B., & Thorne, R. M. (1993). On the preferred source location for the convective amplification of ion cyclotron waves. *Journal of Geophysical Research*, *98*(A6), 9233–9247. https://doi.org/10.1029/92JA02972

Horne, R. B., Thorne, R. M., Glauert, S. A., Menietti, J. D., Shprits, Y. Y., & Gurnett, D. A. (2008). Gyro-resonant electron acceleration at Jupiter. *Nature Physics*, *4*(4), 301–304. https://doi.org/10.1038/nphys897

Huang, S. Y., Fu, H. S., Yuan, Z. G., Vaivads, A., Khotyaintsev, Y. V., Retino, A., et al. (2016). Two types of whistler waves in the hall reconnection region. *Journal of Geophysical Research: Space Physics*, *121*, 6639–6646. https://doi.org/10.1002/2016JA022650

Huang, S. Y., Yuan, Z. G., Sahraoui, F., Fu, H. S., Pang, Y., Zhou, M., et al. (2017). Occurrence rate of whistler waves in the magnetotail reconnection region. *Journal of Geophysical Research: Space Physics*, *122*, 7188–7196. https://doi.org/10.1002/2016JA023670

Kennel, C. F., & Petschek, H. E. (1966). Limit on stably trapped particle fluxes. *Journal of Geophysical Research*, *71*(1), 1–28. https://doi.org/10.1029/JZ071i001p00001

Kletzing, C. A., Kurth, W. S., Acuna, M., MacDowall, R. J., Torbert, R. B., Averkamp, T., et al. (2013). The Electric and Magnetic Field Instrument Suite and Integrated Science (EMFISIS) on RBSP. *Space Science Reviews*, *179*(1–4), 127–181. https://doi.org/10.1007/s11214-013-9993-6

Kurth, W. S., De Pascuale, S., Faden, J. B., Kletzing, C. A., Hospodarsky, G. B., Thaller, S., & Wygant, J. R. (2015). Electron densities inferred from plasma wave spectra obtained by the Waves instrument on Van Allen Probes. *Journal of Geophysical Research: Space Physics*, *120*, 904–914. https://doi.org/10.1002/2014JA020857

Li, W., Thorne, R. M., Angelopoulos, V., Bonnell, J. W., McFadden, J. P., Carlson, C. W., et al. (2009). Evaluation of whistler-mode chorus intensification on the nightside during an injection event observed on the THEMIS spacecraft. *Journal of Geophysical Research*, *114*, A00C14. https://doi.org/10.1029/2008JA013554

Li, W., Thorne, R. M., Angelopoulos, V., Bortnik, J., Cully, C. M., Ni, B., et al. (2009). Global distribution of whistler-mode chorus waves observed on the THEMIS spacecraft. *Geophysical Research Letters*, *36*, L09104. https://doi.org/10.1029/2009GL037595

Li, W., Thorne, R. M., Bortnik, J., Shprits, Y. Y., Nishimura, Y., Angelopoulos, V., et al. (2011). Typical properties of rising and falling tone chorus waves. *Geophysical Research Letters*, *38*, L14103. https://doi.org/10.1029/2011GL047925

Li, W., Thorne, R. M., Bortnik, J., Tao, X., & Angelopoulos, V. (2012). Characteristics of hiss-like and discrete whistler-mode emissions. *Geophysical Research Letters*, *39*, L18106. https://doi.org/10.1029/2012GL053206

Li, W., Thorne, R. M., Meredith, N. P., Horne, R. B., Bortnik, J., Shprits, Y. Y., & Ni, B. (2008). Evaluation of whistler mode chorus amplification during an injection event observed on CRRES. *Journal of Geophysical Research*, *113*, A09210. https://doi.org/10.1029/2008JA013129

Liu, K., Gary, S. P., & Winske, D. (2011). Excitation of banded whistler waves in the magnetosphere. *Geophysical Research Letters*, *38*, L14108. https://doi.org/10.1029/2011GL048375

Liu, N., Su, Z., Gao, Z., Zheng, H., Wang, Y., Wang, S., et al. (2017). Simultaneous disappearances of plasmaspheric hiss, exohiss, and chorus waves triggered by a sudden decrease in solar wind dynamic pressure. *Geophysical Research Letters*, *44*, 52–61. https://doi.org/10.1002/2016GL071987

Liu, S., Xiao, F., Yang, C., He, Y., Zhou, Q., Kletzing, C. A., et al. (2015). Van Allen Probes observations linking radiation belt electrons to chorus waves during 2014 multiple storms. *Journal of Geophysical Research: Space Physics*, *120*, 938–948. https://doi.org/10.1002/2014JA020781

Mauk, B. H., Fox, N. J., Kanekal, S. G., Kessel, R. L., Sibeck, D. G., & Ukhorskiy, A. (2013). Science objectives and rationale for the Radiation Belt Storm Probes mission. *Space Science Reviews*, *179*(1–4), 3–27. https://doi.org/10.1007/s11214-012-9908-y

Meredith, N. P., Horne, R. B., Thorne, R. M., Summers, D., & Anderson, R. R. (2004). Substorm dependence of plasmaspheric hiss. *Journal of Geophysical Research*, *109*, A06209. https://doi.org/10.1029/2004JA010387

Olsen, R. C., Shawhan, S. D., Gallagher, D. L., Green, J. L., Chappell, C. R., & Anderson, R. R. (1987). Plasma observations at the Earth's magnetic equator. *Journal of Geophysical Research*, *92*(A3), 2385–2407. https://doi.org/10.1029/JA092iA03p02385

Omura, Y., Katoh, Y., & Summers, D. (2008). Theory and simulation of the generation of whistler-mode chorus. *Journal of Geophysical Research*, *113*, A04223. https://doi.org/10.1029/2007JA012622

Russell, C. T., Zhang, T. L., Magnes, M., Strangeway, R. J., & Wei, H. Y. (2007). Lightning on Venus inferred from whistler-mode waves in the ionosphere. *Nature*, *450*(7170), 661–662. https://doi.org/10.1038/nature05930

Santolík, O., Gurnett, D. A., Pickett, J. S., Parrot, M., & Cornilleau-Wehrlin, N. (2003). Spatiotemporal structure of storm-time chorus. *Journal of Geophysical Research*, *108*(A7), 1278. https://doi.org/10.1029/2002JA009791

Seough, J., & Yoon, P. H. (2012). Quasilinear theory of anisotropy-beta relations for proton cyclotron and parallel firehose instabilities. *Journal of Geophysical Research*, *117*, A08101. https://doi.org/10.1029/2012JA017645

Shprits, Y. Y., Subbotin, D., Drozdov, A., Usanova, M. E., Kellerman, A., Orlova, K., et al. (2013). Unusual stable trapping of the ultrarelativistic electrons in the Van Allen radiation belts. *Nature Physics*, *9*(11), 699–703. https://doi.org/10.1038/nphys2760

Su, Z., Zhu, H., Xiao, F., Zheng, H., Wang, Y., He, Z., et al. (2014). Intense duskside lower band chorus waves observed by Van Allen Probes: Generation and potential acceleration effect on radiation belt electrons. *Journal of Geophysical Research: Space Physics*, *119*, 4266–4273. https://doi.org/10.1002/2014JA019919

Summers, D., Ma, C., Meredith, N. P., Horne, R. B., Thorne, R. M., Heynderickx, D., & Anderson, R. R. (2002). Model of the energization of outer-zone electrons by whistler-mode chorus during the October 9, 1990 geomagnetic storm. *Geophysical Research Letters*, *29*(24), 2174. https://doi.org/10.1029/2002GL016039

Summers, D., Ni, B., Meredith, N. P., Horne, R. B., Thorne, R. M., Moldwin, M. B., & Anderson, R. R. (2008). Electron scattering by whistler-mode ELF hiss in plasmaspheric plumes. *Journal of Geophysical Research*, *113*, A04219. https://doi.org/10.1029/2007JA012678

Summers, D., Tang, R., & Omura, Y. (2011). Effects of nonlinear wave growth on extreme radiation belt electron fluxes. *Journal of Geophysical Research*, *116*, A10226. https://doi.org/10.1029/2011JA016602

Thorne, R. M., Li, W., Ni, B., Ma, Q., Bortnik, J., Chen, L., et al. (2013). Rapid local acceleration of relativistic radiation-belt electrons by magnetospheric chorus. *Nature*, *504*(7480), 411–414. https://doi.org/10.1038/nature12889

Thorne, R. M., Ni, B., Tao, X., Horne, R. B., & Meredith, N. P. (2010). Scattering by chorus waves as the dominant cause of diffuse auroral precipitation. *Nature*, *467*(7318), 943–946. https://doi.org/10.1038/nature09467

Thorne, R. M., Smith, E. J., Burton, R. K., & Holzer, R. E. (1973). Plasmaspheric hiss. *Journal of Geophysical Research*, *78*(10), 1581–1596. https://doi.org/10.1029/JA078i010p01581

Thorne, R. M., Smith, E. J., Fiske, K. J., & Church, S. R. (1974). Intensity variation of ELF hiss and chorus during isolated substorms. *Geophysical Research Letters*, *1*(5), 193–196. https://doi.org/10.1029/GL001i005p00193

Tsurutani, B. T., & Smith, E. J. (1977). Two types of magnetospheric ELF chorus and their substorm dependences. *Journal of Geophysical Research*, *82*(32), 5112–5128. https://doi.org/10.1029/JA082i032p05112

Xiao, F., Su, Z., Zheng, H., & Wang, S. (2009). Modeling of outer radiation belt electrons by multidimensional diffusion process. *Journal of Geophysical Research*, *114*, A03201. https://doi.org/10.1029/2008JA013580

Xiao, F., Su, Z., Zheng, H., & Wang, S. (2010). Three-dimensional simulations of outer radiation belt electron dynamics including cross-diffusion terms. *Journal of Geophysical Research*, *115*, A05216. https://doi.org/10.1029/2009JA014541

Xiao, F., Yang, C., He, Z., Su, Z., Zhou, Q., He, Y., et al. (2014). Chorus acceleration of radiation belt relativistic electrons during March 2013 geomagnetic storm. *Journal of Geophysical Research: Space Physics*, *119*, 3325–3332. https://doi.org/10.1002/2014JA019822

Xiao, F., Yang, C., Su, Z., Zhou, Q., He, Z., He, Y., et al. (2015). Wave-driven butterfly distribution of Van Allen belt relativistic electrons. *Nature Communications*, *6*(1), 8590. https://doi.org/10.1038/ncomms9590

Xiao, F., Zhou, Q., Zheng, H., & Wang, S. (2006). Whistler instability threshold condition of energetic electrons by kappa distribution in space plasmas. *Journal of Geophysical Research*, *111*, A08208. https://doi.org/10.1029/2006JA011612

Yang, C., Xiao, F., He, Y., Liu, S., Zhou, Q., Guo, M., & Zhao, W. (2018). Storm time evolution of outer radiation belt relativistic electrons by a nearly continuous distribution of chorus. *Geophysical Research Letters*, *45*, 2159–2167. https://doi.org/10.1002/2017GL075894

Yu, X., Yuan, Z., Huang, S., Yao, F., Wang, D., Funsten, H. O., & Wygant, J. R. (2018). Excitation of O^+ band EMIC waves through H^+ ring velocity distributions: Van Allen Probe observations. *Geophysical Research Letters*, *45*, 1271–1276. https://doi.org/10.1002/2018GL077109

Yu, X., Yuan, Z., Wang, D., Huang, S., Qiao, Z., Yu, T., & Yao, F. (2016). Excitation of oblique O^+ band EMIC waves in the inner magnetosphere driven by hot H^+ with ring velocity distributions. *Journal of Geophysical Research: Space Physics*, *121*, 11,101–11,112. https://doi.org/10.1002/2016JA023221

Yuan, Z., Xiong, Y., Pang, Y., Zhou, M., Deng, X., Trotignon, J. G., et al. (2012). Wave-particle interaction in a plasmaspheric plume observed by a Cluster satellite. *Journal of Geophysical Research*, *117*, A03205. https://doi.org/10.1029/2011JA017152

Yuan, Z., Yu, X., Huang, S., Wang, D., & Funsten, H. O. (2017). In situ observations of magnetosonic waves modulated by background plasma density. *Geophysical Research Letters*, *44*, 7628–7633. https://doi.org/10.1002/2017GL074681